In-medium effects on K^0 mesons in relativistic heavy-ion collisions

G. Agakishiev,[8] A. Balanda,[3,21] B. Bannier,[5] R. Bassini,[9] D. Belver,[15] A. V. Belyaev,[6] A. Blanco,[2] M. Böhmer,[11] J. L. Boyard,[13] P. Cabanelas,[15] E. Castro,[15] S. Chernenko,[6] T. Christ,[11] M. Destefanis,[8] J. Díaz,[16] F. Dohrmann,[5] A. Dybczak,[3] T. Eberl,[11] E. Epple,[17] L. Fabbietti,[17,*] O. V. Fateev,[6] P. Finocchiaro,[1] P. Fonte,[2,18] J. Friese,[11] I. Fröhlich,[7] T. Galatyuk,[4] J. A. Garzón,[15] R. Gernhäuser,[11] A. Gil,[16] C. Gilardi,[8] M. Golubeva,[10] D. González-Díaz,[4] F. Guber,[10] M. Gumberidze,[13] M. Heilmann,[7] T. Heinz,[4] T. Hennino,[13] R. Holzmann,[4] I. Iori,[9,20] A. Ivashkin,[10] M. Jurkovic,[11] B. Kämpfer,[5,19] K. Kanaki,[5] T. Karavicheva,[10] D. Kirschner,[8] I. Koenig,[4] W. Koenig,[4] B. W. Kolb,[4] R. Kotte,[5] F. Krizek,[14] R. Krücken,[11] W. Kühn,[8] A. Kugler,[14] A. Kurepin,[10] S. Lang,[4] J. S. Lange,[8] K. Lapidus,[10] T. Liu,[13] L. Lopes,[2] M. Lorenz,[7] L. Maier,[11] A. Mangiarotti,[2] J. Markert,[7] V. Metag,[8] B. Michalska,[3] J. Michel,[7] D. Mishra,[8] E. Morinière,[13] J. Mousa,[12] C. Müntz,[7] L. Naumann,[5] J. Otwinowski,[3] Y. C. Pachmayer,[7] M. Palka,[4] Y. Parpottas,[12] V. Pechenov,[8] O. Pechenova,[8] T. Pérez Cavalcanti,[8] J. Pietraszko,[4] W. Przygoda,[3,21] B. Ramstein,[13] A. Reshetin,[10] M. Roy-Stephan,[13] A. Rustamov,[4] A. Sadovsky,[10] B. Sailer,[11] P. Salabura,[3] A. Schmah,[17,†] E. Schwab,[4] J. Siebenson,[17] Yu. G. Sobolev,[14] S. Spataro,[8,22] B. Spruck,[8] H. Ströbele,[7] J. Stroth,[4,7] C. Sturm,[7] A. Tarantola,[7] K. Teilab,[7] P. Tlusty,[14] M. Traxler,[4] R. Trebacz,[3] H. Tsertos,[12] V. Wagner,[14] M. Weber,[11] C. Wendisch,[5] M. Wisniowski,[3] T. Wojcik,[3] J. Wüstenfeld,[5] S. Yurevich,[4] Y. V. Zanevsky,[6] P. Zhou,[5] and P. Zumbruch[4]

(HADES Collaboration)

[1]*Istituto Nazionale di Fisica Nucleare—Laboratori Nazionali del Sud, I-95125 Catania, Italy*

[2]*LIP-Laboratório de Instrumentação e Física Experimental de Partículas, P-3004-516 Coimbra, Portugal*

[3]*Smoluchowski Institute of Physics, Jagiellonian University of Cracow, 30-059 Kraków, Poland*

[4]*GSI Helmholtzzentrum für Schwerionenforschung GmbH, D-64291 Darmstadt, Germany*

[5]*Institut für Strahlenphysik, Forschungszentrum Dresden Rossendorf, D-01314 Dresden, Germany*

[6]*Joint Institute of Nuclear Research, 141980 Dubna, Russia*

[7]*Institut für Kernphysik, Johann Wolfgang Goethe-Universität, D-60438 Frankfurt, Germany*

[8]*II.Physikalisches Institut, Justus Liebig Universität Giessen, D-35392 Giessen, Germany*

[9]*Istituto Nazionale di Fisica Nucleare, Sezione di Milano, I-20133 Milano, Italy*

[10]*Institute for Nuclear Research, Russian Academy of Science, 117312 Moscow, Russia*

[11]*Physik Department E12, Technische Universität München, D-85748 München, Germany*

[12]*Department of Physics, University of Cyprus, 1678 Nicosia, Cyprus*

[13]*Institut de Physique Nucléaire (UMR 8608), CNRS/IN2P3—Université Paris Sud, F-91406 Orsay Cedex, France*

[14]*Nuclear Physics Institute, Academy of Sciences of Czech Republic, 25068 Rez, Czech Republic*

[15]*Departamento de Física de Partículas, Univ. de Santiago de Compostela, E-15706 Santiago de Compostela, Spain*

[16]*Instituto de Física Corpuscular, Universidad de Valencia-CSIC, E-46971 Valencia, Spain*

[17]*Excellence Cluster Universe, Technische Universität München, Boltzmannstr.2, D-85748 Garching, Germany*

[18]*ISEC Coimbra, Coimbra, Portugal*

[19]*Technische Universität Dresden, D-01062 Dresden, Germany*

[20]*Dipartimento di Fisica, Università di Milano, I-20133 Milano, Italy*

[21]*Panstwowa Wyzsza Szkola Zawodowa, 33-300 Nowy Sacz, Poland*

[22]*Dipartimento di Fisica Generale, Università di Torino, I-10125 Torino, Italy*

C. Hartnack

Subatech, Ecole des Mines, 4 rue A. Kastler F-44307 Nantes, France

(Received 22 April 2010; published 29 October 2010)

We present the transverse momentum spectra and rapidity distributions of π^- and K^0_S in Ar + KCl reactions at a beam kinetic energy of 1.756 A GeV measured with the High Acceptance Di-Electron Spectrometer (HADES). The reconstructed K^0_S sample is characterized by good event statistics for a wide range in momentum and rapidity. We compare the experimental π^- and K^0_S distributions to predictions by the Isospin Quantum Molecular Dynamics (IQMD) model. The model calculations show that K^0_S at low transverse momenta constitute a particularly well-suited tool to investigate the kaon in-medium potential. Our K^0_S data suggest a strong repulsive in-medium K^0 potential of about 40 MeV strength.

DOI: 10.1103/PhysRevC.82.044907 PACS number(s): 25.75.Dw

I. INTRODUCTION

Heavy ion collisions at relativistic energies in the Schwerionen Synchrotron (SIS) energy regime ($E = 1$–2 A GeV) allow for the creation of rather dense nuclear systems up to a few times the saturation density and this provides a favorable

*laura.fabbietti@ph.tum.de

†alexander.schmah@ph.tum.de

environment for the study of in-medium hadron properties. Within this context, expected medium effects on strange particles have been in the focus of nuclear reaction studies at SIS energies for the past two decades. The predicted appearance of a kaon condensate in compressed nuclear matter [1] with its consequences for the understanding of neutron star evolution [2] has emphasized the quest for a quantitative determination of the kaon-nucleon/nucleus potential. So far, particular efforts have been devoted to the production of K^+ and K^- mesons and have provided phase-space distributions, integral yields, and angular distributions for a wide range of energies and collision systems.

The systematics of the experimental K^+ observables and, in particular, the results from sideward [3] and out-of-plane [4] flow analyses suggest a repulsive kaon-nucleus potential. Data from proton-induced reactions support a moderately repulsive potential for K^+ of the order of 20 MeV [5,6], in agreement with theoretical calculations [7–10].

Results concerning the K^- [5] are hampered by the low statistics available and no settled quantitative conclusions can be drawn so far about the strength of the attractive potential.

Neutral kaons can shed additional light on the underlying question. They have the advantage that possible medium effects are not obscured by the Coulomb interaction. Similar to K^+, the K^0 in-medium potential is expected to be repulsive at these energies as can be inferred from recent results extracted from pion-induced reactions [11]. Indeed, the comparison of the K^0_S momentum distribution in the $\pi^- + C$ and $\pi^- + Pb$ reaction points to the existence of a repulsive KN potential of 20 ± 5 MeV at a normal nuclear density.

In this article we report on results for π^- and K^0_S extracted from Ar + KCl reactions at 1.756 A GeV. The high statistics data sample covers almost the entire phase space and allows a detailed analysis of the low-momentum component. For the first time, p_t distributions for K^0_S down to 50 MeV/c for the whole rapidity range can be measured. The study of the low-momentum region is well suited to access the K^0 potential in the nuclear medium since there repulsive effects are expected to show up in a more pronounced way. Moreover, the spectral shape of the p_t distribution allows quantitative conclusions, without requiring any absolute normalization necessary for descriptions that rely on measured yields only. The obtained K^0_S data are compared to our results obtained for K^+ [12] and to theoretical calculations by the Isospin Quantum Molecular Dynamics (IQMD) transport model [13] leading to an estimate of the strength of the repulsive K^0 in-medium potential.

Our article is organized as follows. Section II summarizes the experiment and Sec. III addresses aspects of the particle identification method. This section presents also transverse mass spectra and rapidity distributions for π^- mesons including a comparison to IQMD results. Section IV is devoted to the K^0_S reconstruction procedure based on $\pi^-\pi^+$ pair decays. In Sec. V we contrast the obtained K^0_S distributions to K^+ data measured in the same reaction and compare them to the results of IQMD simulations. In this section we discuss the findings concerning the K^0 in-medium potential. We close with a summary in Sec. VI.

II. THE EXPERIMENT

The experiment was performed with the High Acceptance Di-Electron Spectrometer (HADES) at the heavy-ion synchrotron SIS at GSI Helmholtzzentrum für Schwerionenforschung in Darmstadt, Germany. A detailed description of the spectrometer is presented in Ref. [14].

HADES consists of a six-coil toroidal magnet centered on the beam axis and six identical detection sections located between the coils and covering polar angles from 18° to 85°. In the measurement presented here, the six sectors comprised a gaseous ring-imaging Cherenkov (RICH) detector, four planes of multiwire drift chambers (MDC's) for track reconstruction and two time-of-flight walls (TOF and TOFino), supplemented at forward polar angles with preshower chambers. For each sector, the TOF and TOFino/preshower detectors are combined to a multiplicity and electron trigger array (META).

An $^{40}_{18+}$Ar beam of $\sim 10^6$ particles/s was incident on a four-fold segmented KCl target with a total thickness corresponding to a 3.3% interaction length. A fast diamond start detector located upstream of the target was used to determine the interaction time. The data readout was started by a first-level trigger (LVL1) decision, requiring an observed charged-particle multiplicity MUL $\geqslant 16$ in the TOF/TOFino detectors, accepting approximately 35% of the nuclear reaction cross section. This centrality selection translates into an average participants number $A_{\text{part}} = 38.5 \pm 2.7$, as described in Refs. [12,15].

III. PION IDENTIFICATION

The reconstruction of $K^0_S \to \pi^-\pi^+$ decays requires a clean and unambiguous pion identification within the high multiplicity track ensemble of each event. Charged particles fire wires in the MDC's in front and behind the magnetic field and one or more hits in the META detector. In the so-called cluster finder software [14,16] track-segments are formed using the information from the two pairs of MDC planes. In the track-segment fitting procedures possible trajectories through the two track segments and the META hits are calculated. For a detailed description of the tracking procedure see Refs. [12,17]. After proper correlation of track segments and META hit points, particle momenta were calculated with a Runge-Kutta integration of the trajectory in the magnetic field. The graphical cuts utilized to select the $\pi^\pm$ sample on the base of the dE/dx versus momentum distributions are the same as shown in Ref. [12]. This selection allows us to extract a high-purity pion sample. Muons from pion decays ($\pi^\pm \to \mu^\pm + \nu_\mu$, $BR = 99,9\%$, $c\tau = 7.8$ m) inside the HADES spectrometer constitute only a small fraction of the tracks and are mostly misidentified as pions due to their small mass difference. Hence the effective losses are in the order of a few percent only, as shown in Ref. [18].

The efficiency of the MDC-dE/dx cut and the purity of the selected sample were extracted from the experimental data, selecting particles fully reconstructed in the spectrometer and identified by the META as a reference and then verified using simulations, applying to the simulated tracks the same selection criteria as for the real data. The average efficiencies,

defined as the fraction of real pions surviving all the cuts are ≃90%. The purity of this sample also corresponds to ≃90%. While these values are rather independent of particle momentum for π^- mesons, a significant reduction of the purity is observed for π^+ with momenta $p \geqslant 400$ MeV/c due to contamination by misidentified protons. However, the K^0_S reconstruction is only very weakly affected by the purity of the high-momentum π^+ sample. The acceptance of the HADES spectrometer and the efficiency of the $\pi^\pm$ reconstruction were determined by a full-scale GEANT3 [19] simulation. A sample of pions generated with a flat distribution in rapidity ($-0.75 < y_{\text{c.m.}} < 0.75$) and transverse mass ($0 < m_t - m_\pi < 550\ \text{MeV/c}^2$) was propagated through the whole spectrometer yielding the geometrical acceptance from registered detector hits. The detection efficiency of the pion sample was obtained from the ratio of all emitted tracks inside the acceptance to fully reconstructed tracks subjected to the same selection criteria as for the experimental data.

IV. PION RESULTS

Reduced transverse mass distributions for π^- are shown in Fig. 1 for different center of mass rapidities [$y_{\text{c.m.}} = y - y(\text{c.m.}), y(\text{c.m.}) = 0.86$]. The data are corrected for the efficiency and the spectrometer acceptance and are normalized to the number of LVL1 triggers. The representation per transverse mass and rapidity unit divided by m_t^2 is chosen to ease the comparison with a Boltzmann distribution. A fit

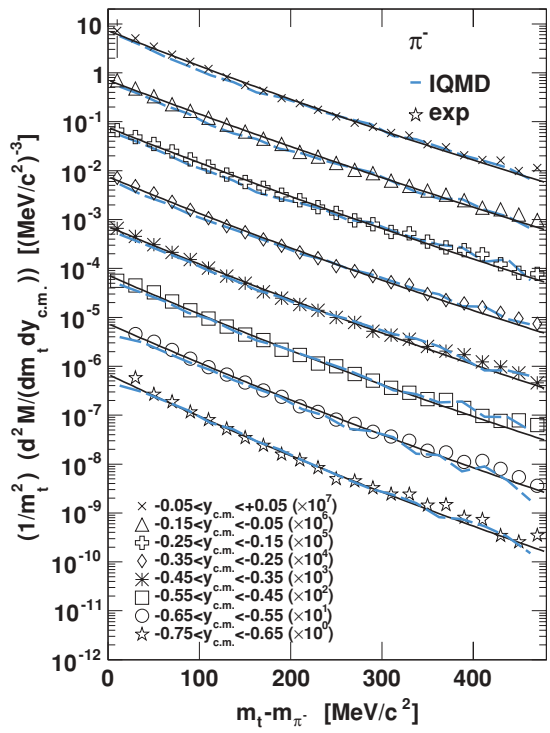

FIG. 1. (Color online) Reduced transverse mass distribution for different rapidity bins for the backward hemisphere for π^- together with predictions by the IQMD model (dashed lines) and the fit (full lines) of the experimental data (symbols).

according to

$$\frac{1}{m_t^2}\frac{d^2M}{dm_t dy} = C(y)\exp\left(-\frac{(m_t - m_0)c^2}{T_B(y)}\right), \qquad (1)$$

was applied to the $m_t - m_\pi$ distribution in two adjacent m_t intervals. The pions mainly stem from the decay of the $\Delta(1232)$ resonance and are produced at different stages of the collision with varying "hardness" as time proceeds. Hence the measured π spectrum is a superposition of different Δ generations. This explains why a single Boltzmann fit (1) is not sufficient to match the data. It was found that a simultaneous two-slope Boltzmann fit with the transverse mass intervals chosen as $0 < m_t - m_\pi < 180\ \text{MeV/c}^2$ and $180 < m_t - m_\pi < 500\ \text{MeV/c}^2$, reproduces the data adequately. The two m_t ranges have been first fitted with two independent Boltzmann distributions yielding the start parameter values for the simultaneous fit. For the latter, the start values were allowed to vary up to a maximum of 10%. The resulting Boltzmann distributions are plotted in Fig. 1 as solid lines.

As already shown in Ref. [20], measured pion spectra can be reproduced reasonably well by IQMD calculations [21–27]. The present HADES data are compared to IQMD calculations assuming a hard cut on the impact parameter $b < 6$ fm, which corresponds to a number of participants of 38.5 ± 4.6. The π^- m_t distributions obtained for the experimental data (symbols) are shown in Fig. 1 for different $y_{\text{c.m.}}$ bins together with the IQMD calculations (dashed lines) assuming the centrality selection $b < 6$ fm. The same fitting procedure was applied to the IQMD data points. The obtained inverse slope parameters $T_{1,2}$ for the experimental and simulated data are shown in Fig. 2 as a function of rapidity $y_{\text{c.m.}}$. We observe a systematic difference of 10–15% between the slope factor T_1 determined in the forward and backward rapidity hemispheres, which is not present in T_2. The agreement between the data and model is of similar quality.

The full curves shown in Fig. 2 represent a fit to the experimental data according to

$$T_B(y) = \frac{T_{\text{eff}}}{\cosh(y - y_{\text{c.m.}})}, \qquad (2)$$

that allows us to extract the effective slopes for the pion in the two m_t ranges. The obtained values $T_{\text{eff}1,2}$ are shown in the two panels of Fig. 2.

Transverse momentum spectra of pions in Ar + KCl collisions at a very similar energy (1.808 A GeV) have been published as kinetic-energy spectra at 90° in the center-of-mass frame [28], which corresponds to midrapidity. The comparison with our data after proper normalization to the same number of participant nucleons shows agreement within the quoted errors.

The functions resulting from the fits to the pion transverse-mass distributions in the different rapidity bins in Fig. 1 are integrated over the interval $0 < m_t - m_\pi < \infty$ to obtain the yields as a function of rapidity. This integration method is justified by the large coverage of the experimental $m_t - m_\pi$ distribution and the good agreement between the data and the fit function. The resulting rapidity distribution of π^- is displayed in Fig. 3 together with the values obtained

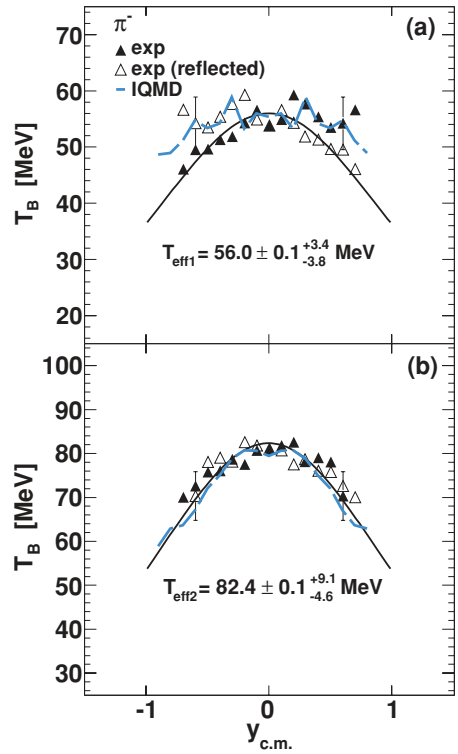

FIG. 2. (Color online) (a) Rapidity dependence of slope parameters obtained by fitting the π^- m_t distributions from experimental data (full symbols) and IQMD simulations (dashed curve) in the range $0 < m_t - m_\pi < 180$ MeV/c^2. (b) Slope parameters obtained fitting the same distribution in the range $180 < m_t - m_\pi < 500$ MeV/c^2. The values of the effective slopes $T_{\text{eff}1/2}$ were obtained by employing function (2).

integrating the IQMD distributions. The two distributions are in agreement within 15%; the largest deviation shows up in the midrapidity range. The total yield of negatively charged pions was calculated from a Gaussian fit to the dN/dy distribution shown in Fig. 3. The systematic error on the pion multiplicity has been estimated varying the boundaries used as start values for the transverse mass fits in the range from 120 to 300 MeV/c^2 and repeating for each step

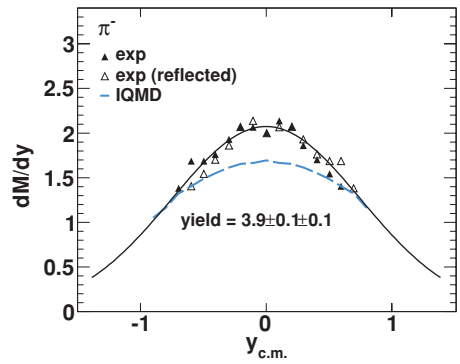

FIG. 3. (Color online) Rapidity distribution of π^- experimental data and reflected data points around midrapidity (full and empty triangles) together with the result from the IQMD calculation (dashed curve). The full curve shows a Gaussian fit of the experimental data.

the same fitting procedure described previously. We obtain $M_{\text{exp}}(\pi^-) = 3.9 \pm 0.1 \pm 0.1$ and $M_{\text{IQMD}}(\pi^-) = 3.7$, which are compatible within the error. Any systematic error derived from the comparison of the backward and forward distributions was found to be smaller than the statistical error. These results were confirmed by an independent analysis in Ref. [15]. Taking as a reference the pion multiplicities estimated in Ref. [20] for the Ar + KCl system at 1.756 GeV, agreement is achieved as well.

A comparison with earlier data and the IQMD model that is independent of the trigger details and impact parameter selection is possible by normalizing the pion yield to the number of participating nucleons. For the data presented here we find $\langle N_\pi \rangle / A_{\text{part}} = 0.101 \pm 0.003 \pm 0.008$ (where the last error contains the uncertainty of the calculation of the A_{part}value with UrQMD, ≈7%). From IQMD we get $\langle N_\pi \rangle / A_{\text{part}} = 0.105 \pm 0.015$. From Ref. [28] for $\langle N_\pi \rangle = 5.6$ and $A_{\text{part}} = 60$ we obtain 0.093.

V. K^0_S RECONSTRUCTION

The K^0_S meson (mean decay length $c\tau = 2.7$ cm) decays into a $\pi^+ + \pi^-$ pair with a branching ratio of 69%. After the selection of events with two identified pion tracks, the invariant mass was calculated for each $\pi^+ - \pi^-$ combination. To reduce the combinatorial background from uncorrelated $\pi^+ - \pi^-$ pairs and hence to enhance the purity of the K^0_S signal, various cuts on characteristic geometrical distances have been applied: (1) the minimum distance between the two pion tracks ($d_{\pi^+-\pi^-} < 10$ mm), (2) the distance of closest approach to the primary vertex for the two pion tracks [$d_0(\pi^+, \pi^-) \geqslant 6$ mm and $d_0(K^0_S) < 10$ mm], and (3) the distance between the primary reaction and secondary decay vertex [$d(K^0_S - V) \geqslant 30$ mm]. The method is discussed in detail in Ref. [17]. Figure 4 (top) shows the resulting invariant-mass distribution of all $\pi^+ - \pi^-$ pairs. The peak corresponding to the K^0_S signal is clearly visible on the top of the background which is reproduced using the mixed-event technique (dashed area in the top of Fig. 4). For the background analysis, only those events were chosen for which the individual pion tracks originate from the same target segment of the four-fold KCl target stack.

The resulting K^0_S signal after background subtraction is shown in Fig. 4 (bottom) and it can be fitted by the sum of two Gaussian distributions. A rather sharp distribution that contains most of the yield and a broader distribution that corresponds to the case where at least one of the two pions has undergone multiple scattering. The Gaussian fit in Fig. 4 shows the result for the sharper distribution and corresponds to the following mean value and dispersion for the reconstructed mass $\langle m_{K^0_S} \rangle = 492.5$ MeV/c^2 and $\langle \sigma_{K^0_S} \rangle = 9.3$ MeV/c^2. The width of the reconstructed signal and the signal-to-background ratio depend on the rapidity bin and vary in the range 7 MeV/c^2 $< \sigma_{K^0_S} <$ 12.4 MeV/c^2 and $0.3 < S/B < 2.0$, respectively. A total of about 65.700 K^0_S mesons are identified in an interval of $\pm 3\sigma$ around the fitted mass peak.

The phase-space distribution of the measured K^0_S is shown in Fig. 5 as a function of the reduced transverse mass $m_t - m_{K^0_S}$

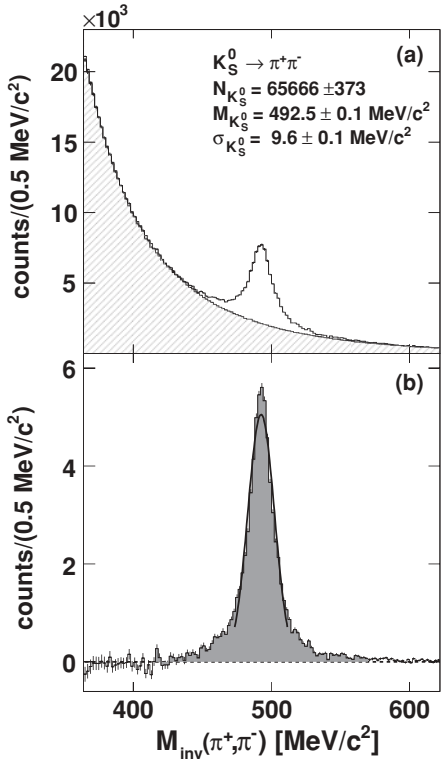

FIG. 4. Invariant-mass distribution of $\pi^+ - \pi^-$ pairs (a). The combinatorial background (shaded area) is obtained by the mixed-event technique. The background-subtracted distribution (b) shows clearly the K^0_S meson signal (grey area with a Gaussian fit).

and center-of-mass rapidity $y_{\text{c.m.}}$. From the plot it is evident that the low transverse momentum region is covered with significant statistics for the whole rapidity range.

For the quantitative analysis, acceptance and efficiency corrections have been applied to the reconstructed K^0_S signal in a similar way as described for the single $\pi^\pm$ tracks in Sec. III. A K^0_S event generator with a flat distribution in rapidity ($-0.75 < y_{\text{c.m.}} < 0.75$) and transverse mass ($0 < m_t - m_{K^0_S} < 900\ \text{MeV}/c^2$) was used as the input of a full-scale

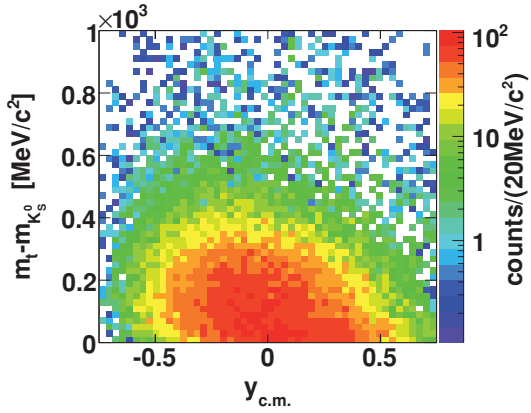

FIG. 5. (Color online) Distribution of the reconstructed K^0_S yield as a function of the subtracted transverse mass $m_t - m_{K^0_S}$ and the center-of-mass rapidity $y_{\text{c.m.}}$. The color code refers to the number of kaons per bin.

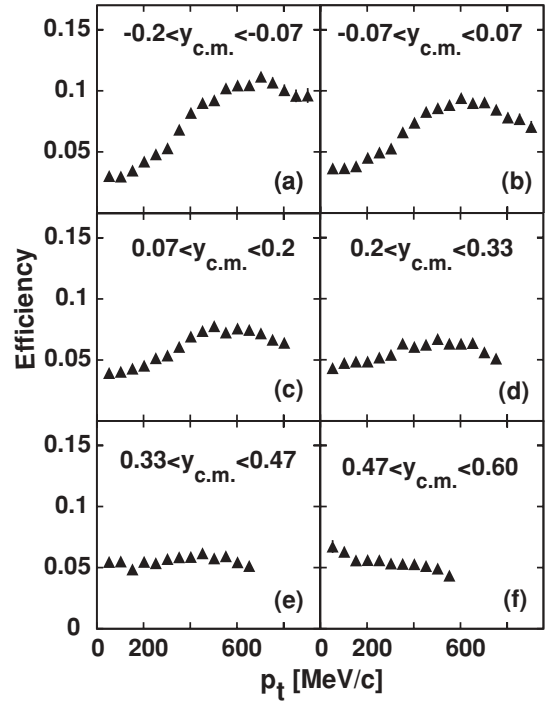

FIG. 6. K^0_S reconstruction efficiency as a function of the transverse momentum p_t and for different rapidity bins. The geometrical acceptance is not taken into account.

simulation to evaluate the geometrical acceptance and the reconstruction efficiency. The average geometrical acceptance for K^0_S amounts to 20–25% [17], the reconstruction efficiency to ≃5–10%. The latter is shown in detail in Fig. 6 as a function of the transverse momentum p_t for different rapidity bins. In addition, the branching ratio of the decay $K^0_S \to \pi^+ + \pi^-$ was corrected for.

VI. K^0_S RESULTS

A. Transverse mass spectra

The K^0_S transverse mass spectra obtained after background subtraction and correction for acceptance and efficiency are plotted in Fig. 7 (open symbols) for various $y_{\text{c.m.}}$ bins together with the K^+ spectra (full symbols). Since in isospin symmetric heavy-ion reactions the yields of K^+ and K^0 should be the same and since the K^- yield is negligible compared to the K^+ yield we have $K^+ + K^- = K^0 + \bar{K}^0 = K^0_S + K^0_L = 2 \cdot K^0_S$. For this reason, the data for the K^+ mesons (full symbols) in Fig. 7 were multiplied by a factor of 0.5. The quantitative comparison of these experimental spectra that are found to be in good agreement is a valuable cross check of the analysis. Neglecting final state Coulomb interactions, the dynamics of the interaction between K^+ and K^0 mesons and the nuclear medium should result in similar kinematic distributions.

Using the Boltzmann parametrization (1), an inverse slope parameter $T_B(y)$ can be determined as a function of the rapidity. The dashed lines in Fig. 7 shows the Boltzmann fit-functions. The resulting $T_B(y)$ values as a function of the rapidity obtained from the fit of the K^0_S data are shown in Fig. 8 together with the results obtained for the K^+ [12] and

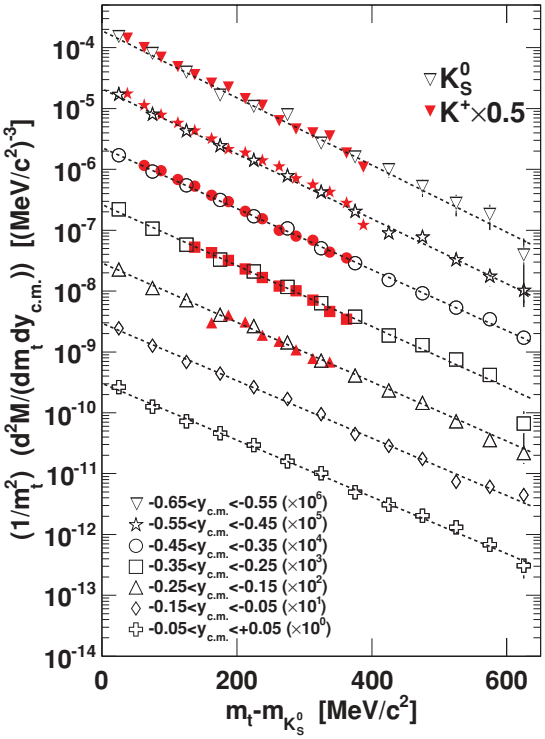

FIG. 7. (Color online) Transverse mass spectrum for different center-of-mass rapidity bins, corresponding to the backward hemisphere only, for K^0_S (empty symbols), K^+ multiplied by a factor of 0.5 (full symbols), and fits assuming a Boltzmann parametrization (dashed lines).

by the IQMD simulations. The two curves in Fig. 8 refer to two different scenarios: (1) no in-medium potential (dotted lines in Fig. 9) and (2) a repulsive potential of 40 MeV (dashed lines). Fitting the $T_B(y)$ distribution with the function (2), the parameter $T_{\rm eff}$ can be extracted. It represents the inverse slope at midrapidity and corresponds to an effective temperature at the kinetic freeze-out stage.

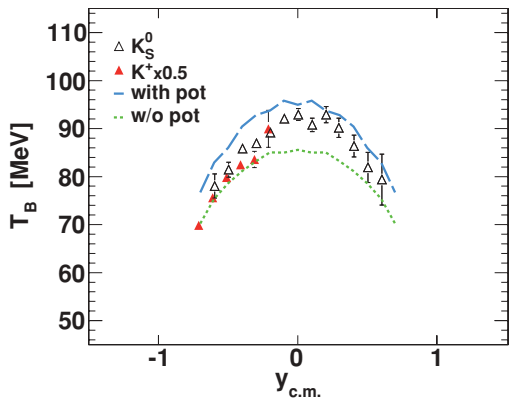

FIG. 8. (Color online) Rapidity dependence of slope parameters obtained by fitting the K^0_S and K^+ m_t distributions from experimental data (empty and full symbols, respectively). The results by IQMD simulations employing a repulsive potential (dashed curve) and no potential (dotted curve) are shown as well. The errors are statistical only.

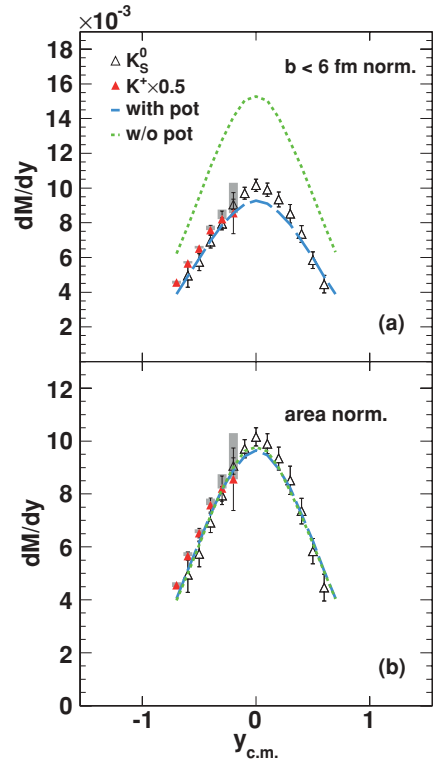

FIG. 9. (Color online) Rapidity distribution of K^0_S (empty triangles) and K^+ mesons (full triangles from Ref. [12]) together with the distributions obtained with the IQMD calculation assuming a repulsive (dashed line) and no (dotted line) potential for two different normalization procedures (panels a and b, see text for details). The vertical boxes show the systematic errors associated to the K^+ data.

The averaged $T_{\rm eff}$ for K^0_S is found to be 92 ± 2 MeV which agrees within the errors with the findings for K^+ in the same data set [12].

B. Rapidity distribution

The fitted K^0_S invariant transverse mass distributions are integrated within the whole interval $0 < m_t - m_{K^0_S} < \infty$ to obtain the meson yield per rapidity unit. To evaluate the precision of this integration, the integral of the fitting function was compared to the integrated data points in the range $0 < m_t - m_{K^0_S} < 600$ MeV/c^2. We find an agreement between 0.5 and 2.5% for all rapidity bins, except for the interval $-0.65 < y_{\rm c.m.} < -0.55$ for which the difference amounts 6.5%.

The resulting rapidity distribution is shown in Fig. 9 (empty symbols), together with the respective K^+ yields divided by a factor two (full symbols). The systematic error of the K^0_S yield has been estimated by varying the geometrical cuts and the track quality selection in several combinations. The systematic errors shown for the K^+ distribution have been calculated as described in Ref. [12]. Both experimental distributions overlap within the error bars. Appropriate integration yields a total K^0_S multiplicity of $(1.15 \pm 0.05 \pm 0.09) \cdot 10^{-2}$ as compared to a total K^+ multiplicity of $(2.8 \pm 0.2 \pm 0.1 \pm 0.1) \cdot 10^{-2}$ [12], where the first and second (third) errors are the statistical and systematic, respectively. The differences in the tails of the

rapidity distributions shown in Fig. 9 lead to slightly different 4π yields. Nevertheless, the multiplicities, extracted with two independent analyses, agree within the error, confirming the quality of the K^0_S data.

Together with the experimental distributions, the IQMD results for the same two scenarios presented in Fig. 8 are shown. In the top panel of Fig. 9 the IQMD calculations ($b < 6$ fm) without any normalization are shown, while in the bottom panel the two curves are shown after a normalization to the total area of the experimental distribution. The IQMD calculation used here corresponds to the standard setting with $\alpha = 1.0$ (see Sec. VI C) already shown in Refs. [10,29].

Although the standard parametrization used in the previous IQMD calculations were successfully used for comparison to KaoS and FOPI data and thus supports the results of this comparison, a direct conclusion on the optical potential from absolute yields is premature. It was shown in Ref. [30] that transport models using opposite assumptions on the optical potential but different parametrizations of poorly known production cross sections were able to reproduce the same rapidity distribution of kaons in central Ni + Ni events at 1.93 A GeV measured by FOPI and KaoS.

The calculations with and without potential have indeed very similar shapes (bottom panel of Fig. 9). The rapidity distribution contains the integrated information about p_t and assuming that the effect of the potential is momentum dependent, the differential study of the p_t distribution can add important information. The study of the p_t distributions between 50 and 800 MeV/c constitutes the key clue of our approach to determine the in-medium K^0 potential, as described in the following section.

C. Comparison with IQMD

As shown in Sec. III, the IQMD calculations are in reasonably good agreement with the pion spectra measured for the Ar + KCl reaction at 1.756 A GeV as far as the slopes are concerned, but differ up to 15% in the absolute yield. These findings impose a caveat on the absolute normalization of the IQMD simulations on the experimental data. Starting with the same centrality selection used to obtain the pion spectra ($b < 6$ fm), a set of calculations with the IQMD model [13] has been carried out, employing a repulsive K^0-nucleus potential of varying strength.

According to Ref. [31], $K^+ = \bar{s}u$ is a "good" quasiparticle with narrow width; the same is expected for $K^0 = \bar{s}d$. Its dispersion relation may be written as $\omega^2 = m_K^2 + k^2 + \Pi$ with $\omega(k)$ as energy (momentum) and Π as real part of the self-energy. The latter one accounts for the influence of the ambient medium, thus leading to an effective in-medium mass $m* = \omega(k = 0)$. According to the low density theorem, both the K^0 and K^+ mass should increase in nuclear matter. Another way to state this is to say that the kaons interact with the surrounding nucleons via a Schrödinger-type potential. An increase of $m*$ is thereby related to a repulsive total potential. The easiest parametrization is the linear Ansatz $m* = m_\rho + U(\alpha)\rho/\rho_0$ where $\rho(\rho_0)$ is the nuclear matter (saturation) density. For the IQMD settings [13], the parameter

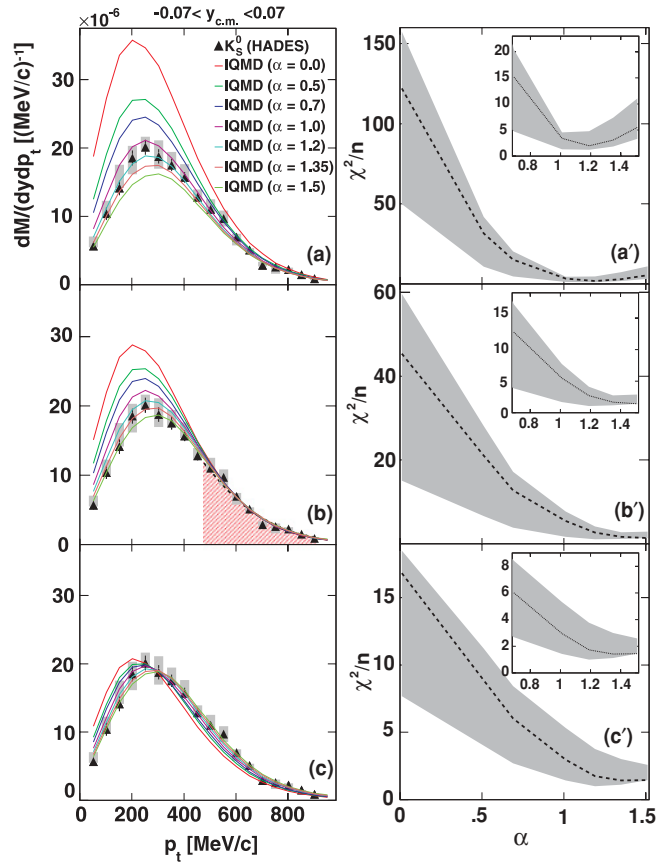

FIG. 10. (Color online) Left panels: p_t distributions of K^0_S at mid-rapidity (full symbols) compared with different calculations by the IQMD model. The different solid curves correspond to a variation of the parameter α, which couples directly to the potential strength. The comparison is shown for three different normalization procedures (see text for details). Right panels: Normalized χ^2 distribution as a function of the parameter α extracted from the comparison of the IQMD calculations to the experimental data for three different normalization procedures (see text for details). The insets show a zoom around the minimum of the distribution.

α is related to the potential U via $U(\alpha) \simeq U_0 + U'\alpha$ with $U_0 \approx 0.8$ MeV and $U' \approx 38$ MeV [13].

To evaluate more quantitatively the comparison between the IQMD and experimental data, we have first focused on the midrapidity p_t distribution and compared systematically the experimental data with different IQMD calculations obtained varying the parameter α. The left panels of Fig. 10 show the K^0_S p_t distribution at midrapidity, together with the results of the IQMD calculations for different values of the parameter α. The three panels correspond to three different ways of normalization of the IQMD calculations to the experimental data. Figure 10(a) shows the case where the IQMD curves for $b < 6$ fm have not been normalized to the data, Fig. 10(b) shows the case where all the IQMD curves have been normalized to the high-p_t tail ($p_t > 475$ MeV/c) of the experimental distribution and Fig. 10(c) shows the case where the area underlying each curve has been normalized to the integral of the experimental distribution. The error shown for the experimental data contains also the systematic contribution.

This contribution was evaluated varying the cuts for the K^0_S selection for 14 different combinations. A χ^2 analysis was carried out applying a best fit of the different IQMD curves to the experimental data. The results corresponding to the three normalization procedures are shown in panels (a′), (b′), and (c′) of Fig. 10 where the error bands include both the statistical and systematic contributions. The inlets in the three panels show a zoom on the minimum region. The minimum of the χ^2 distribution that corresponds to an optimal set of cuts for the K^0_S is obtained for the following α values, respectively: 1.13–0.12, 1.37–0.2, and 1.34–0.17.

The asymmetric error on α was evaluated taking the minimum χ^2 value + 1 for each of the 14 different χ^2 distributions and reading the corresponding α value on the left side of the minimum. The maximal deviation of this value from the minimum of the dashed curves was assigned to the asymmetric error. Since IQMD calculations corresponding to α values higher than 1.5 lead to unphysical results, it is not possible to calculate the upper value of the α parameter.

One can see that even considering the three normalization methods simultaneously the lowest limit for α is 1, which corresponds to a minimum repulsive potential of 38.7 MeV.

It also has to be mentioned that the IQMD calculations quoted in Ref. [29], which interpret the whole K^+ KaoS systematics in favor of a soft Earth Observing System (EOS) but do not draw any conclusions on the potential, used $\alpha = 1.0$ as well.

This rather high value of the extracted potential is larger that the results reported in Refs. [3,5,9,11,32], which reported a value of 20 ± 5 MeV. However, the potential values extracted so far from K^0_S data are derived from $\pi^- + A$ reactions [11]. In this case the pion absorption happens on the nucleus surface so that many of the produced kaons do not travel through the nucleus. Furthermore, the HADES data deliver higher statistics and accuracy in the measurement of the low p_t range, which is more sensitive to the potential effects. Also, the results extracted from K^+ data in proton-induced reactions [32] test subnormal nuclear density and cannot be directly compared with the data from heavy-ion collisions where average densities of 1.5–2 ρ_0 are reached. Overall the nuclear environment resulting in the Ar + KCl reaction can lead to a stronger repulsive potential for K^0.

However, as extensively discussed in Refs. [10,33], the different transport codes that have been employed to interpret the available data on kaons differ substantially in their implementation, in their elementary production cross sections, and in their treatment of the parameters connected to the strength of the potential. To get a consistent picture, the HADES K^0_S data can be described by other models and the interpretation of the K^+ data previously measured in heavy-ion collisions [3] might be revised using updated versions of theoretical models and elementary cross sections [33].

Taking as a reference the IQMD simulation corresponding to $\alpha = 0$ and $\alpha = 1.2$, we compared them to the experimental p_t distributions as shown in Fig. 11. The left panels of Fig. 11 show the K^0_S p_t distributions for different rapidity bins, together with the IQMD calculations assuming either no repulsive potential (dotted curves) or a potential of about 46.1 MeV ($\alpha = 1.2$, dashed curves). For this comparison the simulations

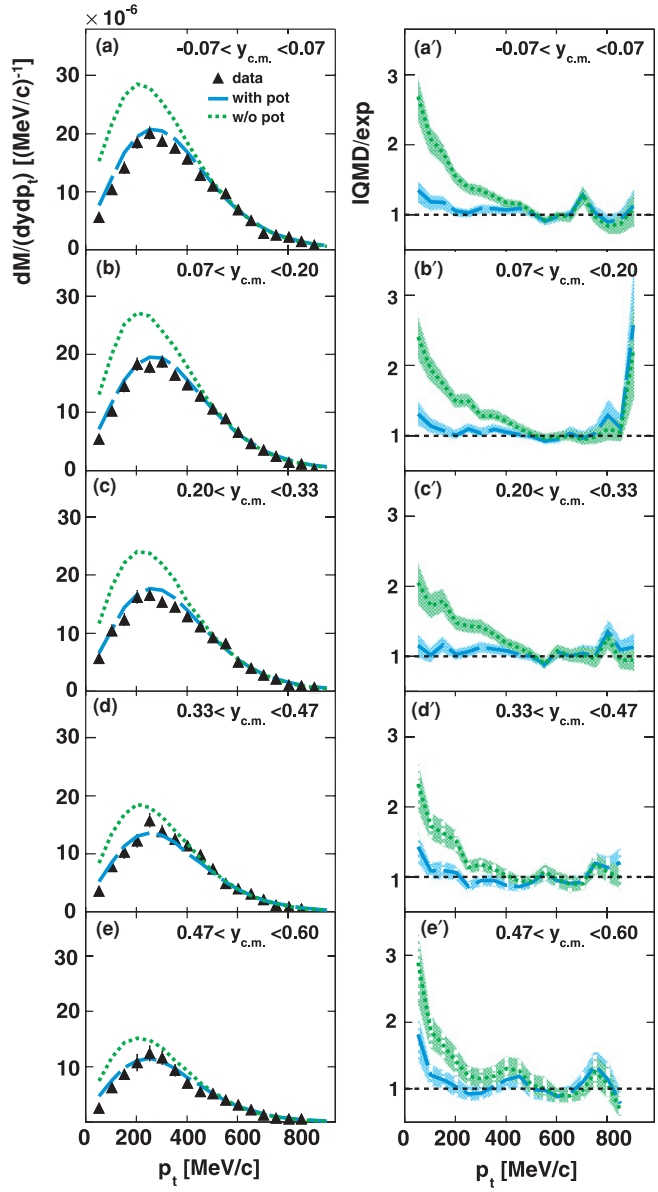

FIG. 11. (Color online) Left panels: p_t distribution of the experimental K^0_S data (full triangles) together with the yields calculated by the IQMD model including a repulsive K^0-nucleus potential of 46.1 MeV (dashed curves) and without potential (dotted curves) for different rapidity bins. Right panels: ratio between the calculation by the IQMD model and the experimental data as a function of p_t for different rapidity bins.

are normalized to the high-momentum tail of the experimental distribution starting from $p_t = 475$ MeV/c since in this region the effect of the repulsive potential should be negligible. The displayed errors are only statistical. On the right panels of Fig. 11, the ratio of the simulated to experimental yield is displayed for the two cases with and without a repulsive potential. The error band displayed for the ratios are again only statistical.

It is very interesting to notice that the IQMD simulation assuming a repulsive potential agrees rather well with the experimental data for all the rapidity bins. The calculations

without the potential, however, overestimate the experimental data, especially in the low transverse momentum regime (<400 MeV/c), as is clearly visible in the ratio plots. This behavior is slightly more evident at midrapidity but persists with the same trend for the whole rapidity range.

We note that the p_t spectra exhibit the most sensitive dependence on the K^0-nucleus potential. The rapidity distribution is sensitive to variations of the quantity α as well, but this effect is less pronounced and the conclusions drawn on the potential strength are strongly dependent upon the normalization of the simulated to experimental data. Hence the accurate study of the p_t spectra delivers a new more powerful tool to extract quantitative information.

VII. SUMMARY

Rapidity and transverse momentum spectra of π^- and K^0_S mesons produced in Ar + KCl collisions at 1.756 A GeV and measured with HADES were investigated. For the first time in this energy regime, K^0_S spectra have been measured with high statistics and precision in almost the full phase space and, in particular, down to low momenta ($p_{\min} \approx 50$ MeV/c).

The π^- data were shown and compared quantitatively to IQMD calculations, using an absolute normalization based on the selection of the impact parameter $b < 6$ fm in the simulations and a centrality selection on the experimental data corresponding to the most central 35% of the total cross section. The π^- rapidity density distribution shows a quantitative agreement with the IQMD model within 15%.

For K^0_S mesons the transverse mass and the rapidity density distribution are compared to previously published K^+ data and agree well with them, both in shape and yield. The comparison of the K^0_S rapidity distribution with IQMD calculations does not seem to be solid enough to extract reliable information about the potential since the normalization is not certain and the calculations corresponding to different values of the potential deliver curves with the same shape. The K^0_S p_t distributions were found to be a better observable and were compared to calculations by the IQMD model assuming different strengths of the K^0-nuclear medium potential. This comparison supports the existence of a rather strong repulsive potential of about 40 MeV. These data are now available for further studies via the available transport models.

ACKNOWLEDGMENTS

We gratefully acknowledge the useful discussions with J. Aichelin and H. Oeschler. The HADES collaboration gratefully acknowledges the support by BMBF Grant Nos. 06TM970I, 06GI146I, 06FY171, and 06DR135 (Germany), by GSI (TM-FR1, GI/ME3, OF/STR), by Excellence Cluster of Universe (Germany), by Grant Nos. GA AS CR IAA100480803 and MSMT LC 07050 (Czech Republic), by Grant No. KBN 5P03B 140 20 (Poland), by INFN (Italy), by CNRS/IN2P3 (France), by Grant Nos. MCYT FPA2000-2041-C02-02 and XUGA PGID T02PXIC20605PN (Spain), by Grant No. UCY-10.3.11.12 (Cyprus), by INTAS Grant No. 06-1000012-8861 and EU Contract No. RII3-CT-2004-506078.

[1] D. B. Kaplan and A. E. Nelson, Phys. Lett. B **175**, 57 (1986).
[2] E. E. Kolomeitsev, D. N. Voskresensky, and B. Kämpfer, Nucl. Phys. A **588**, 889 (1995).
[3] P. Crochet *et al.* (FOPI Collaboration), Phys. Lett. B **486**, 6 (2000).
[4] Y. Shin *et al.* (KaoS Collaboration), Phys. Rev. Lett. **81**, 1576 (1998).
[5] W. Scheinast *et al.* (KaoS Collaboration), Phys. Rev. Lett. **96**, 072301 (2006).
[6] D. Best *et al.* (FOPI Collaboration), Nucl. Phys. A **625**, 307 (1997).
[7] E. Bratkovskaya *et al.*, Nucl. Phys. A **622**, 593 (1997).
[8] G. Q. Li *et al.*, Phys. Lett. B **381**, 17 (1996).
[9] Z. Rudy *et al.*, Eur. Phys. J. A **23**, 379 (2005).
[10] C. Fuchs, Prog. Part. Nucl. Phys. **56**, 1 (2006).
[11] M. L. Benabderrahmane *et al.* (FOPI Collaboration), Phys. Rev. Lett. **102**, 182501 (2009).
[12] G. Agakishiev *et al.* (HADES Collaboration), Phys. Rev. C **80**, 025209 (2009).
[13] C. Hartnack and J. Aichelin, private communication.
[14] G. Agakichiev *et al.* (HADES Collaboration), Eur. Phys. J. A **41**, 243 (2009).
[15] P. Tlusty *et al.* (HADES Collaboration), in *Proceedings of the XLVII International Winter Meeting on Nuclear Physics, Bormio (Italy)*, Jan. 26–30, 2009.
[16] J. Markert, Ph.D. thesis, University of Frankfurt, 2005.
[17] A. Schmah, Ph.D. thesis, University of Darmstadt, 2008.
[18] G. Agakishiev *et al.* (HADES Collaboration), Eur. Phys. J. A **40**, 45 (2009).
[19] GEANT3.21, Detector Description and Simulation Tool, [http://consult.cern.ch/writeup/geant/] (1993).
[20] W. Reisdorf *et al.* (FOPI Collaboration), Nucl. Phys. A **781**, 459 (2007).
[21] C. Hartnack *et al.*, Eur. Phys. J. A **1**, 151 (1998).
[22] J. Aichelin, Phys. Rep. **202**, 233 (1991).
[23] S. A. Bass, C. Hartnack, R. Mattiello, H. Stöcker, and W. Greiner, Phys. Lett. B **302**, 381 (1993).
[24] S. A. Bass, C. Hartnack, H. Stöcker, and W. Greiner, Phys. Rev. C **50**, 2167 (1994).
[25] S. A. Bass, M. Hofmann, C. Hartnack, H. Stöcker, and W. Greiner, Phys. Lett. B **335**, 289 (1994).
[26] S. A. Bass, C. Hartnack, H. Stöcker, and W. Greiner, Phys. Rev. C **51**, 3343 (1995).
[27] S. A. Bass, C. Hartnack, H. Stöcker, and W. Greiner, Phys. Rev. C **51**, R12 (1995).
[28] A. Sandoval *et al.*, Phys. Rev. Lett. **45**, 874 (1980).
[29] A. Förster *et al.* (KaoS Collaboration), Phys. Rev. C **75**, 024906 (2007).
[30] C. Hartnack and J. Aichelin, J. Phys. G **28**, 1649 (2002).
[31] C. L. Korpa and M. Lutz, Acta Phys. Hung. A **22**, 21 (2005).
[32] M. Nekipelov *et al.* (ANKE Collaboration), Phys. Lett. B **540**, 207 (2002).
[33] E. E. Kolomeitsev *et al.*, J. Phys. G **31**, S741 (2005).